GANIT

Available online at https://ganitjournal.bdmathsociety.org/

GANIT: Journal of Bangladesh Mathematical Society

GANIT *J. Bangladesh Math. Soc.* 41.1 (2021) 62–77
DOI: https://doi.org/10.3329/ganit.v41i1.55027

Arterial pharmacokinetics in a patient-specific atherosclerotic artery-a simulation study

Sayantan Biswas[a], Sarifuddin[b], and Prashanta Kumar Mandal *[c]

[a,c] *Department of Mathematics, Visva Bharati University, Santiniketan-731 235, West Bengal, India*
[b] *Department of Mathematics, Berhampore College, Berhampore-742 101, West Bengal, India*

ABSTRACT

Of concern in the paper is a numerical study of endovascular drug delivery in a patient-specific atherosclerotic artery through a mathematical model in which the luminal flow is governed by an incompressible viscous Newtonian fluid, and the transport of luminal as well as tissue concentration is modeled as an unsteady convection-diffusion process. An image processing technique has been successfully adopted to detect the edges of the computational domain extracted from an asymmetric (about the centerline of the artery) patient-specific atherosclerotic artery. Considering each pixel as a control volume, the Marker and Cell (MAC) method has been leveraged to get a quantitative insight of the model considered by exploiting physiologically realistic initial, boundary as well as interface conditions. Simulated results reveal that the number as well as the length of separation zone does increase with increasing Re, and the near-wall velocity contour might be important for estimating the near-wall residence time for the pool of drug molecules available for tissue uptake. Results also show that the more the tissue porosity and interface roughness do not necessarily imply the more the effectiveness of delivery, even though they enhance the averaged concentration in the tissue domains, and also the area under concentration diminishes with increasing Peclet number. Thus, the tissue porosity, the Peclet number and various geometrical shapes (interface roughness) play a pivotal role in the dispersion and the effectiveness of drug delivery.

Received: June 21, 2021 **Accepted:** July 20, 2021 **Published Online:** August 04, 2021

Keywords: Patient-specific asymmetric atherosclerotic artery; Endovascular delivery; Image processing; Marker and Cell Method; Flow separation; Tissue content
AMS Subject Classifications 2020: 35Q35, 92B05, 92C45.

1 Introduction

Constriction in an artery occurs due to the accumulation of low-density lipoprotein (LDL) and other macromolecules and/or the proliferation of smooth muscle cells (SMCs) present in *tunica media* along the inner lining of the arterial wall. The formation of such constriction or plaque (stenosis) starts blocking the artery and reduces the normal flow of blood, medically termed as 'atherosclerosis'[1]. The study of disturbances arising out of atherosclerotic flow together with its control is a much-researched topic for the last few decades, however,

*Corresponding author. *E-mail address:* prashantakumar.mandal@visva-bharati.ac.in

the convection as well as diffusion-driven transport of drug in a patient-specific atherosclerotic artery has been paid less attention, perhaps due to its inherent complexity in the geometry. During intravenous delivery into an atherosclerotic artery, clinicians are interested to analyze how the luminal drug is dispersed with the flowing blood and its subsequent uptake into the arterial tissue, and also the tissue content for the better efficacy of the delivery.

A large volume of work on the transport of luminal concentration (solute) in the presence of an absorbing wall (lumen-wall interface) has already been carried out, both theoretically and/or numerically, in various domains of interest [2, 3, 4, 5, 6, 7, 8, 9]. Taylor [2] and Aris [3] studied the solute dispersion in steady flow through a circular tube. Gill and Sankarasubramanian [4] carried out the exact analysis of an unsteady convection-diffusion process. In their study, a fully developed steady laminar flow and the dispersion of an injected solute in each time without interphase mass transfer across boundaries were analyzed. A more rigorous generalization was derived by taking the key attributes of solute transfer in the presence of an absorbing boundary [5]. The effect of wall absorption on shear dispersion in plane and pipe flows was successfully studied by Smith [6]. Purnama [7] considered the dispersion of solute between a moving region and adjoining immobile medium. Dash et al. [8] explored the effect of yield stress on solute dispersion in Casson fluid flow. The study of Sarkar and Jayaraman [9], taking annular and axisymmetric oscillatory flow consecutively into account, was based on irreversible boundary reaction on the dispersion of solute. **Nagarani et al. [10]** analyzed the dispersion process in a tube in the presence of a catheter. The investigation on the mass transport contemplated a steady Poiseuille flow through a circular tube considering reversible and irreversible reactive boundary condition [11]. In the presence of reversible and irreversible wall reaction in an annular tube with an oscillatory flow, Mazumder and Paul [12] analyzed the longitudinal dispersion following Aris's method of moments. Rana and Murthy [13, 14] analytically determined the transport coefficients with the help of Gill's generalized dispersion model and discussed the effect of yield stress, wall reaction, Womersley parameter and flow pulsatility on the dispersion of solute in a tube and in two-phase flow respectively. Three layers of fluid having non-Newtonian Casson model in the middle layer were considered to investigate the effect of yield stress, the thickness of the layer and wall reaction on solute transport using the Aris-Barton method of moments by Debnath et al. [15].

In all the studies cited above, studies on the solute transport were restricted only in the luminal region. It is surprising to know that the transport of solute in the lumen as well as in the tissue is not well documented so far. Few studies have considered the transport of solute followed by its absorption at the lumen-tissue interface in an idealized (non-realistic and smooth having no surface roughness) wall [16, 17]. In a theoretical study, Griffiths et al.[16] made an attempt to optimize the mass transport in a thin porous tube. Since the therapeutic domain is an atherosclerotic artery, Das et al. [17] successfully simulated the dispersion of solute in an idealized stenotic artery. They showed that the dispersion of solute in the lumen and the tissue is directly related to the yield stress, the wall absorption parameter and the severity of the stenosis. It is well established that the uptake of solute from the luminal side depends on the near-wall velocity gradient. Some studies showed the alteration of flow characteristics in presence of surface irregularities by disregarding the solute transport in the tissue [18, 19, 20, 21, 22, 23, 24]. These studies, though less flexible, are still of relevance to establish the effects of roughness on solute transport. Studies related to drug delivery in various geometries have been successfully carried out in the recent past [25, 26, 27].

Relatively very little is known about the drug transport in the vicinity of a realistic atherosclerotic artery. An issue of central interest in the present study is the consideration of irregular lumen-tissue interfaces which promote multi-directional drug uptake from the luminal side as opposed to the smooth interface. In this work, a longitudinal image of an asymmetric patient-specific atherosclerotic arterial segment obtained from intravascular ultrasound (IVUS) is taken into consideration [28]. An image processing technique was successfully applied to obtain the outlines of the computational domain [29]. For a quantitative insight of this coupled fluid-drug transport model considering the continuity of flux and concentration as the lumen-tissue interface, the well-known Marker and Cell method is leveraged [30] where each pixel of the longitudinal image is considered as a control volume. It may be recorded that this asymmetric geometry consisting varying irregularities at the upper and lower interfaces contributes much to the varying uptake of drug therein. Our study differs considerably from the studies cited above by taking additional consideration of an unsteady drug transport in tissue domains having varying lumen-tissue interface roughness in the upper and lower domains. The transport of drug molecules with the streaming blood in the lumen after injected at the luminal inlet and its subsequent uptake at the irregular lumen-tissue interface followed by diffusion in the tissue is relevant in the study of arterial pharmacokinetics. The objective of the present computational study is to investigate the convective and diffusive transport of drug in an irregular asymmetric patient-specific atherosclerotic artery and to estimate various physiological factors like velocity, wall shear stress, pressure drop, streamlines, concentration in their respective irregular domains as

well as the effectiveness of delivery. The novelty of the present study lies in the inclusion of a patient-specific asymmetric atherosclerotic artery with varying irregularities at the lumen-tissue interfaces and the dispersion of the drug molecules in the lumen and tissue in general, and the choice of solute administration at the luminal inlet for three different geometrical models which more closely resembles the physiological situation relevant to intravenous drug delivery. The possible implications of the results are discussed.

2 Formulation of the Problem

2.1 Geometry Reconstruction

The three different models of an atherosclerotic vessel shown in Fig. 1 (a-c) have been examined. The 'Original' shape considered here is the patient-specific asymmetric model (Fig 1(c)) [28]. The 'Toy' model considered is a much simpler smooth version of the original shape (Fig. 1(a)). Finally, by gradually adding interface roughness to the toy model, a new stenosis model, termed as 'Smooth' model, is obtained which exhibits the same general form as the original model with few surface roughness elements are present (Fig. 1(b)). The computational domain for the original model was constructed from a single, patient-specific asymmetric arterial vessel obtained from König and Klauss [28]. In this case, intravascular ultrasound (IVUS) imaging was performed to obtain a longitudinal cross-section of the vessel followed by virtual histology on the derived image to identify the outlines of the computational domain. An image segmentation technique was leveraged to automatically identify different outlines of the image [29]. IVUS is a tomographic imaging tool that allows visualization of atherosclerosis, its length and area, plaque compositions and coronary remodeling. The motivation of selecting this image is simply due to its availability and it allows us to define boundary and interface conditions straightforwardly. **We limited our formulation in a two-dimensional geometry of an asymmetric patient-specific atherosclerotic artery due to its availability in the literature [28].**

2.2 Governing Equations

Although blood, being a suspension of enumerable corpuscles, behaves like a non-Newtonian fluid while flowing through smaller vessels, but in larger arteries, the rheology of the streaming blood may be treated as Newtonian [31]. In our study, the luminal blood flow is treated as unsteady and two-dimensional which is characterized by Newtonian model. The dimensionless governing equations representing the trasport of momentum (eqns. 1,2) and conservation of mass (eqn. 3) for viscous incompressible fluid in Cartesian coordinates system (x, y) may be written in the conservative form as

$$\frac{\partial u}{\partial t} + \frac{\partial (\mathbf{uv})}{\partial y} + \frac{\partial u^2}{\partial x} = -\frac{1}{\rho}\frac{\partial p}{\partial x} - \frac{1}{Re}\left(\frac{\partial^2 u}{\partial x^2} + \frac{\partial^2 u}{\partial y^2}\right), \tag{2.1}$$

$$\frac{\partial v}{\partial t} + \frac{\partial v^2}{\partial y} + \frac{\partial (\mathbf{uv})}{\partial x} = -\frac{1}{\rho}\frac{\partial p}{\partial y} - \frac{1}{Re}\left(\frac{\partial^2 v}{\partial x^2} + \frac{\partial^2 v}{\partial y^2}\right), \tag{2.2}$$

$$\frac{\partial u}{\partial x} + \frac{\partial v}{\partial y} = 0, \tag{2.3}$$

where x and y are the dimensionless coordinates, scaled with respect to the proximal diameter d of the artery with the x axis placed along the centreline of the asymmetric artery, u and v are the axial and the transverse components of dimensionless velocity scaled with the centreline velocity U_0 respectively. Here, ρ represents the density of flowing blood and μ, the viscosity coefficient. The dimensionless time (t), the pressure (p) may be defined as

$$t = \frac{U_0 t^*}{d}, p = \frac{p^* d}{\mu U_0}.$$

Here, $Re(= \frac{\rho U_o d}{\mu})$ stands for the Reynolds number.

The respective convection-diffusion equations representing the transport of drug in the domains considered, namely, the lumen, the upper tissue and the lower tissue, may be written in dimensionless forms as

$$\frac{\partial c_l}{\partial t} + u\frac{\partial c_l}{\partial x} + v\frac{\partial c_l}{\partial y} = \frac{1}{Pe_l}\left(\frac{\partial^2 c_l}{\partial x^2} + \frac{\partial^2 c_l}{\partial y^2}\right), \tag{2.4}$$

$$\frac{\partial c_{tu}}{\partial t} + V_{filt}\frac{\partial c_{tu}}{\partial y} + = \frac{1}{Pe_{tu}}\left(\frac{\partial^2 c_{tu}}{\partial x^2} + \frac{\partial^2 c_{tu}}{\partial y^2}\right), \tag{2.5}$$

$$\frac{\partial c_{tl}}{\partial t} + V_{filt}\frac{\partial c_{tl}}{\partial y} + = \frac{1}{Pe_{tl}}\left(\frac{\partial^2 c_{tl}}{\partial x^2} + \frac{\partial^2 c_{tl}}{\partial y^2}\right), \tag{2.6}$$

where the volume-averaged concentrations of free drug in the lumen(c_l), in the upper tissue(c_{tu}) and in the lower tissue(c_{tl}) are scaled with respect to the inlet concentration c_0. Here, $V_{filt}(= \frac{v_{filt}}{U_o})$ represents the dimnesionless tranmural filtration velocity in the upper and lower tissue regions and $Pe_l(= \frac{U_0 d}{D_l})$,$Pe_{tu}(= \frac{U_0 d}{D_{tu}})$, $Pe_{tl}(= \frac{U_0 d}{D_{tl}})$ stand for the Peclet number for the lumen, the upper tissue and the lower tissue respectively, with the diffusion coefficients D_l in the lumen, D_{tu} in the upper tissue, D_{tl} in the lower tissue.

2.3 Initial, Boundary and lumen-tissue Interface Conditions

An asymmetric velocity profile at the inlet(Γ_i) may be taken as

$$u = \frac{(y - R_u)(y - R_l)}{(R_m - R_u)(R_m - R_l)},\ v = 0 \ \text{ on } \ \Gamma_i, \tag{2.7}$$

where R_i $(i = u, l)$ be the proximal lumen radii (upper and lower) of the arterial segment and $R_m(= \frac{R_u + R_l}{2})$ is the mean radius at the luminal inlet.
At the downstream (Γ_o), the flow is left free which is mathematically represented by

$$\frac{\partial u}{\partial x} = 0 = \frac{\partial v}{\partial x} \text{ on } \Gamma_o. \tag{2.8}$$

At the lumen-tissue interfaces (Γ_i^u, Γ_i^l), the usual no-slip condition of velocity-vector is given by

$$u = 0 = v \ \text{ on } \Gamma_i^u, \Gamma_i^l. \tag{2.9}$$

At the proximal(Γ_p^u, Γ_p^l) and distal (Γ_d^u, Γ_d^l) boundaries of the tissue domains, the no flux conditions for free drug are as follows:

$$\frac{\partial c_{tu}}{\partial x} = 0 \text{ on } \Gamma_p^u, \Gamma_d^u, \tag{2.10}$$

$$\frac{\partial c_{tl}}{\partial x} = 0 \text{ on } \Gamma_p^l, \Gamma_d^l. \tag{2.11}$$

At the perivascular end(Γ_u, Γ_l), a perfectly sink condition may be written mathematically as [16]

$$c_{tu} = 0 \text{ on } \Gamma_u, \tag{2.12}$$

$$c_{tl} = 0 \text{ on } \Gamma_l. \tag{2.13}$$

At the lumen-tissue interfaces (Γ_i^u, Γ_i^l), the continuity of drug concentrations and fluxes are assumed whose mathematical representations are as [16]

$$c_{tu} = c_l \text{ and } \frac{\partial c_l}{\partial \mathbf{n}} = \alpha_1 \frac{\partial c_{tu}}{\partial \mathbf{n}} \text{ on } \Gamma_i^u, \tag{2.14}$$

$$c_{tl} = c_l \text{ and } \frac{\partial c_l}{\partial \mathbf{n}} = \alpha_2 \frac{\partial c_{tl}}{\partial \mathbf{n}} \text{ on } \Gamma_i^l, \tag{2.15}$$

where $\mathbf{n}$ is the transmural unit normal vector, $\alpha_1 = \phi\frac{D_{tu}}{D_l}$ and $\alpha_2 = \phi\frac{D_{tl}}{D_l}$; ϕ designates the porosity of the tissue medium. Due to nonavailability of data, equal porosity and equal diffusivity for both the tissue regions have been assumed, and hence we assume, in the sequel, $\alpha_1 = \alpha_2 = \alpha$. Initially, it is assumed that there is no drug inside the domains (lumen and tissue), except the dimensionless concentration of injected drug at the luminal inlet is constant (unity). Therefore,

$$c_l = 1 \text{ at } x = 0,\ \forall t \text{ and } c_l = c_{tu} = c_{tl} = 0, \text{ elsewhere, at } t = 0 \tag{2.16}$$

3 Method of Solution

3.1 The MAC Methodology

The governing equations along with the physiologically realistic conditions are solved numerically by a finite-difference method in staggered grids. The computational geometry is comprised of 71,876 pixels encompassing the patient-specific atherosclerotic vessel where each pixel is considered as a control volume (Fig. 2). Concerning the second order spatial accuracy of the boundary conditions, some fictitious grid points outside the domain have been taken into consideration. Here, we set $x_i = i\delta x, y_j = j\delta y$ and $t_k = k\delta t$ in which k refers to the time direction, δt, the time increment. Here, δx and δy are the dimensions of the pixels. The discretized versions of the governing equations are not given here, for the sake of brevity, however, the interested readers may be referred to [32]. The discretized equation for calculating pressure-field as obtained from the discretized momentum and continuity equations is solved by Successive-over-Relaxation(SOR) method ehere the value of over-relaxation parameter is 1.2. Using the principle of conservation of mass, we calculate the divergence of the velocity-field at each cell and check for its prescribed tolerance. If the divergence does not satisfy the tolerance limit, then the pressure and velocity components are corrected. The discretized versions of the governing equations are not given here, for the sake of brevity, however, the interested readers may be referred to [32]. The computational code has successfully been programmed in FORTRAN language.

3.2 Pressure and velocity correction

To reduce the computational cost for each cycle, we limit the number of iterations in the S.O.R scheme to 10 to get pressure-field. So the velocity-field obtained using this inaccurate pressure-field will not, in general, satisfy the continuity equation which prompts us to correct the pressure as well as velocity-field. If the cell-divergence is found to be greater than the prescribed tolerance value (10^{-8}) at any cell in an absolute sense, the pressure and, subsequently, the velocity components are immediately corrected at each cell using the formulae below:

$$p^k_{i,j} = p^*_{i,j} + \omega\delta p_{i,j},$$

where $\delta p_{i,j} = \frac{-Div^*_{i,j}}{2\delta t\left(\frac{1}{\delta x^2}+\frac{1}{\delta y^2}\right)}$, $p^*_{i,j}$ is the obtained pressure from the Poisson equation using limited iterations, $\omega(\leq 0.5)$ represents the relaxation parameter for S.O.R. scheme and $Div^*_{i,j}$ stands for derived divergence of the velocity-field at $(i,j)^{\text{th}}$ cell.

$$\begin{aligned} u^{k+1}_{i,j} &= u^*_{i,j} + \frac{\delta t\delta p_{i,j}}{\delta x}, \\ u^{k+1}_{i-1,j} &= u^*_{i-1,j} - \frac{\delta t\delta p_{i,j}}{\delta x}, \\ v^{k+1}_{i,j} &= v^*_{i,j} + \frac{\delta t\delta p_{i,j}}{\delta y}, \\ u^{k+1}_{i,j-1} &= u^*_{i,j-1} - \frac{\delta t\delta p_{i,j}}{\delta y}, \end{aligned}$$

where $u^*_{i,j}, u^*_{i-1,j}, v^*_{i,j}, v^*_{i,j-1}$ stand for the updated velocity-field.

3.3 Numerical Stability: Time-Stepping Procedure

Welch et al.[33] suggested the stability criterion by imposing restriction on time step (δt_1) involving Reynolds number as

$$\delta t_1 \leq \text{Min}\left(\frac{Re}{2}\frac{\delta x^2\delta y^2}{\delta x^2+\delta y^2}\right)_{i,j} \tag{3.1}$$

This condition for stability is related to viscous effect which can be applied directly in order to select an appropriate time step [34].

Another approach for stability criterion is that no fluid particles should cross more than one cell boundary in a given interval of time (δt_2) (Markham and Proctor [35]), which may be written mathematically as

$$\delta t_2 \leq \text{Min}\left(\frac{\delta x}{|u|}, \frac{\delta y}{|v|}\right)_{i,j} \tag{3.2}$$

Courant-Friedrichs-Lewy (CFL) stability criteria [38] based on various diffusivities of the drug and dimension of the control volume provide the time step (δt_3).

Finally, the variable time step (δt) to be applied at a given point in the calculation will be

$$\delta t = d_1 \text{Min}\left(\delta t_1, \delta t_2, \delta t_3\right), \tag{3.3}$$

where the reason for this extra factor d_1, $(0 < d_1 \leq 1)$ is to reduce the computational cost [35].

4 Numerical Results and Discussion

The computational domain is considered of non-dimensional length of 8.5 in which extra non-stenotic lengths at the upstream and downstream are added in a bid to justify the boundary conditions assumed at the proximal and distal end of the arterial segment. The computational domain is comprised of 71,876 pixels encompassing a patient-specific asymmetric atherosclerotic vessel where each pixel is considered as a control volume. Steady states have been achieved when the divergence of the velocity-field was less than 10^{-8} and a reduction of 5.0×10^{-7} in the solute transport residual. For simulation purposes, the following plausible baseline values have been made use of [4, 18, 36, 37]:
$Re = 300, Pe_l = 1000, Pe_{tu} = 10000, Pe_{tl} = 10000, \alpha = 0.1, V_{filt} = \mathcal{O}(10^{-6})$

4.1 Model Validation

Direct validation of our model with ones available in the literature is almost impossible as, to the authors' knowledge, not a single article is available in the literature which accounts for the mass and momentum transport in the domains considered, however, a sincere attempt is made in Figure 3 to qualitatively compare the variation of normalized pressure drop with Reynolds number. The pressure drop is computed across the patient-specific irregular stenosis, and one can easily verify from Fig. 3 that the obtained result does significantly differ from those of [18, 22] who studied the model in cylindrical coordinates system with different plaque geometry, but a similar trend is observed that the predicted pressure drop decreases with increasing Reynolds number. The distinction among these findings is certainly due to the length, the severity and the different irregularities of atherosclerotic plaque considered herein.

4.2 Velocity Contour, Wall Shear Stress and Streamlines

The effect of Reynolds number on the vorticity contours of the flow characteristics in an asymmetric patient-specific atherosclerotic vessel can be recorded from the results of Figure 4. The velocity profiles at the throats are significantly distorted as shown in these patterns. These distortions span downstream with increasing Re. The velocity contours have some interesting features to note that the magnitude of the velocity in the vicinity of the plaque is negative indicating the existence of flow separation regions at those sites and the area of the regions having negative velocity does increase with increasing Re. The correct prediction of the near-wall velocity contour might be important for estimating near-wall residence time for the pool of drug molecules available for tissue uptake. Thus the flow velocity (specifically near the wall) contributes much to the uptake of drug from the luminal side.

The wall shear stress plays a significant role in the genesis and progression of atherosclerosis. The variations of the wall shear stress along the asymmetric as well as irregular vessel for the upper and lower walls for different Re are portrayed in Figure 5(a-b) respectively. The multiple peak values of the wall shear stress occur at the multiple throats of the stenosis and the maximum value is noted where the arterial narrowing is maximum, and also, this peak value increases with increasing Re. It may also be noted that the number, as well as the length of recirculation/ separation region, do increase with increasing Re which may have a pivotal role for the aggravation of the disease (cf. Figs. 6). It is also interesting to note that the number as well as the length of separation zone increases in the upper wall as compared to the lower wall due to more interface irregularities present in the upper interface. Hence, proper importance should be given to the interface irregularities in the context of the atherosclerotic lesion. The elevated wall shear stress is responsible for endothelial damage and activates cellular proliferation mechanism too, and the complex separation regions are responsible for the aggregation sites of macromolecules as opined by Asakura and Karino [39]. The results of Figure 6(a-c) showing patterns of streamlines for an irregular atherosclerotic plaque for different Re clearly indicate that the streamlines are less perturbed for $Re = 100$, however, with an increase of Re, the formation of several complex recirculation regions

is observed due to an increase fluid inertia which is responsible for the establishment of an adverse pressure gradient. This adverse pressure gradient does reverse the flow. The figure also highlights that the streamlines at the lower wall are less perturbed as compared to the upper wall for a particular Re which is due to less surface roughness present in the lower wall. This, however, at least describes quantitatively what happens for flows in blood vessels when the inertia is important. Thus, based on the patterns of the streamlines, one may conclude that the irregularity of the inner lining of the vessel wall affects the streamlines significantly and hence proper importance should be given to the irregular stenosis model in the context of atherosclerotic lesion.

4.3 Effect of diffusivity (Peclet number), tissue porosity (α) and interface roughness on drug dispersion

Figure 7(a-c) exhibits the distributions of local drug concentrations in the axial direction of the atherosclerotic artery at three distinct transluminal positions, namely, $y = 0.2$ for lumen, $y = 1.15$ for upper tissue and $y = -1.15$ for lower tissue, while Figure 8(a-c) displays the spatiotemporal patterns of drug concentration for the whole domain (lumen as well as tissue). Figure 7a shows that the value of the luminal concentration for different luminal Peclet numbers (Pe_l) starts from one due to all-time constant value ($c_l = 1$, eq. 2.16) at the inlet, and thereafter increases followed by a gradual decline at the downstream. Figures 7(b-c) gives an idea on how the local concentration is perturbed for different tissue Peclet numbers (Pe_{tu}, Pe_{tl}). This figure establishes the fact that the drug concentration reduces significantly with the increasing Peclet number. One interesting feature may be noted that the concentration profiles reveal asymmetric distribution between regions distal and proximal to the plaque due to the convective nature of drug transport as well as varying thickness and roughness of the domains. Simulations predicted that recirculation regions create pockets of stagnant drug-laden blood that allow more drug accumulation at lumen-tissue interfaces, and eventually more uptake of drug from the luminal side into the arterial tissue [32]. All these findings are in conformity with the spatiotemporal patterns of drug concentration as depicted in Figure 8(a-c). Here too, the concentration of drug diminishes, more specifically, the area under concentration (AUC) diminishes with increasing Peclet number, and the penetration of drug into the tissue domains is more from the sites of recirculation regions and the more the thickness of the domains, the less the concentration at a particular instant of time.

Temporal variations of averaged concentration of drug for different values of Peclet number and tissue porosity for the upper and lower tissue regions are sketched in Figure 9(a-b) respectively. It is found that the averaged concentration increases from zero, thereafter reaches a steady state with the advancement of time. It is worthwhile to note that the averaged tissue concentration reaches its quasi-steady state more quickly for lesser Peclet number (i.e. for higher diffusivity). As anticipated, the averaged concentration decreases with the increase of Peclet number. Moreover, as the porosity in the tissue α $(= \phi \frac{D_{tu}}{D_l} = \phi \frac{D_{tl}}{D_l})$ increases from 0.05 to 0.1, the averaged concentration of drug in both the tissue domains increases which may be justified in the sense that with the increase of porosity in the tissue, the diffusive flux of luminal concentration into the tissue domain increases, which in turn, diminishes the luminal concentration (cf. Fig. 11(a-c)) and enhances the averaged concentration in the arterial tissue. The averaged concentrations of drug for three different geometrical models (Toy model having no interface roughness, smooth model having few interface roughness and original model having much roughness; cf. Sec. 2.1, Fig. 1(a-c)) for the upper and lower tissue regions are depicted in Figure 10(a-b). The three models differ from each other in terms of interface roughness, and eventually, the length of the interface of the domains changes as the more the roughness present at the interface, the more the lumen-tissue interface length. The curves from both figures are analogous in nature. It is to be noted that the concentration is all-time lower for the toy model, as compared to the smooth and original model for both the tissue domains. This observation makes sense that the smaller interface roughness (interface length) for the toy model gives rise to lesser absorption of drug in the tissue and hence, it may be concluded that the more the interface roughness, the more the absorption of drug, and finally, the more the averaged concentration in the tissue.

4.4 Effect of diffusivity (Peclet number), tissue porosity (α) and interface roughness on the effectiveness of delivery

Following Saltzman [40], the effectiveness of delivery in the target tissue is defined as the ratio of the averaged concentration and maximum concentration. He also opined that the higher value of this ratio implies good effectiveness. Figure 12(a-b) depicts the influence of the Peclet number (diffusivity) and the tissue porosity (α) on the effectiveness of endovascular drug delivery for upper and lower therapeutic domains over time respectively.

As anticipated, the effectiveness of delivery diminishes with increasing Peclet number, which is in tune with the averaged concentration for various Peclet numbers (cf. Fig. 9), but a reverse trend is observed in case of varying porosity. Although the averaged concentration increases with increasing tissue porosity in the upper and lower tissue regions, the effectiveness of delivery decreases. Figure 13(a-b) exhibits the effect of geometrical shape, i.e., interface roughness or interface length on the effectiveness of endovascular drug delivery. Simulated results show that the effectiveness of drug delivery diminishes with increasing interface roughness as opposed to the averaged concentration in both the tissue domains (cf. Fig 10). This observation may be justified in the sense that with the increase of tissue porosity and the interface roughness, the averaged concentration in the tissue domains does increase, but the higher porosity and roughness implying higher tissue uptake of the injected drug give much higher maximum concentration in the tissue, and eventually, the ratio (effectiveness) decreases.

5 Conclusion and future direction

Endovascular delivery through a patient-specific atherosclerotic arterial segment has been considered in the present study. The drug which is transported with the luminal flow and its subsequent uptake into the porous tissue regions clearly resemble intravenous delivery in a realistic situation. **Image processing technique has been successfully used to determine the boundary of the domain of study.** The luminal fluid is modeled as an incompressible Newtonian fluid governed by Navier-Stokes equations. The transport of drug in the lumen and tissue domains are modeled as an unsteady advection-diffusion process. Considering each pixel as a control volume, the Marker and Cell (MAC) method has been leveraged to get a quantitative insight of the model considered by exploiting physiologically realistic initial, boundary as well as interface conditions. Simulated results predict that the number as well as the length of separation zones increases with **increasing** Re **and** the near-wall velocity contour plays a pivotal role for estimating the residence times for the pool of drug molecules available for tissue uptake. One interesting phenomenon may be noted that although the tissue porosity and the interface roughness do enhance the averaged concentration of drug in both the tissue domains, it may not enhance the effectiveness of delivery. Hence, the porosity as well as the interface roughness of the asymmetric therapeutic domains play a pivotal role in the dispersion and the effectiveness of drug delivery.

To model endovascular drug delivery in a complex physiological system is an uphill task, still a sincere attempt is made to study such a problem in a tractable form by making a lot of assumptions. Our model did not consider the rheological effects on dispersion. The consideration of the retention of drug in the therapeutic domains together with its endocytosis (internalization) in the heterogeneous compositions of the plaque may be taken into account in our future endeavor. We intend to revisit these topics mentioned in this section as part of our future research.

Acknowledgement

The authors gratefully acknowledge the research fellowship received from Special Assistance Programme (SAP-III) [Grant No. F.510/3/DRS-III/ 2015 (SAP-I)] sponsored by the University Grants Commission, New Delhi, India.

Conflicts of interest

The authors declare that they have no known competing interest.

References

[1] Ross, R. (1993). Atherosclerosis: a defense mechanism gone awry. The American Journal of Pathology, 143(4), 987–1002.

[2] Taylor, G. I.(1953). Dispersion of a soluble matter in solvent flowing slowly through a tube. Proceedings of the Royal Society of London. Series A. Mathematical and Physical Sciences, 219(1137), 186–203.

[3] Aris, R. (1956). On the dispersion of a solute in a fluid flowing through a tube. Proceedings of the Royal Society of London. Series A. Mathematical and Physical Sciences, 235(1200), 67–77.

[4] Gill, W. N. and Sankarasubramanian, R. (1970). Exact analysis of unsteady convective diffusion. Proceedings of the Royal Society of London. A. Mathematical and Physical Sciences, 316(1526), 341–350.

[5] Sankarasubramanian, R. and Gill, W.N. (1973). Unsteady convective diffusion with inter-phase mass transfer. Proceedings of the Royal Society of London. A. Mathematical and Physical Sciences, 333(1592), 115–132.

[6] Smith, R. (1983). Effect of boundary absorption upon longitudinal dispersion in shear flows. Journal of Fluid Mechanics, 134, 161–177.

[7] Purnama, A. (1988). Boundary retention effects upon contaminant dispersion in parallel flows. Journal of Fluid Mechanics, 195, 393–412.

[8] Dash, R.K., Jayaraman, G. and Mehta, K.N. (2000). Shear augmented dispersion of a solute in a Casson fluid flowing in a conduit. Annals of Biomedical Engineering, 28(4), 373-385.

[9] Sarkar, A. and Jayaraman, G. (2002). The effect of wall absorption on dispersion in annular flows. Acta Mechanica 158, 105-119.

[10] Nagarani, P., Sarojamma, G. and Jayaraman, G. (2006). Exact analysis of unsteady convective diffusion in Casson fluid flow in an annulus–Application to catheterized artery. Acta Mechanica, 187(1-4), 189–202.

[11] Ng, C.O., Rudraiah, N.(2008). Convective diffusion in steady flow through a tube with a retentive and absorptive wall. Physics of Fluids, 20, 073604.

[12] Mazumder, B.S. and Paul, S. (2012). Dispersion of reactive species with reversible and irreversible wall reactions. Heat and Mass Transfer, 48(6), 933-944.

[13] Rana, J., Murthy, P. (2016). Solute dispersion in pulsatile casson fluid flow in a tube with wall absorption. Journal of Fluid Mechanics 793, 877–914.

[14] Rana, J., Murthy, P. (2017). Unsteady solute dispersion in small blood vessels using a two-phase Casson model. Proceedings of the Royal Society A: Mathematical, Physical and Engineering Sciences 473(2204), 20170427.

[15] Debnath, S., Saha, A.K., Mazumder, B., Roy, A.K. (2017). Dispersion phenomena of reactive solute in a pulsatile flow of three-layer liquids. Physics of Fluids 29(9), 097107.

[16] Griffiths, I.M.,Howell, P.D., Shipley, R.J. (2013). Control and optimization of solute transport in a thin porous tube. Physics of Fluids, 25, 033101.

[17] Das, P., Sarifuddin, M. and Mandal, P. K. (2020). Solute dispersion in Casson fluid flow through a stenosed artery with absorptive wall. Zeitschrift Angewandte Mathematik und Physik, 71(3), p.100.

[18] Back, L.H., Cho, Y.I., Crawford, D.W. and Cuffel, R.F. (1984). Effect of mild atherosclerosis on flow resistance in a coronary artery casting of man. ASME Journal of Biomechanical Engineering 106, 48–53.

[19] Johnston, P.R. and Kilpatrick, D. (1991). Mathematical modelling of flow through an irregular arterial stenosis. Journal of Biomechanics, 24(11),1069-1077.

[20] Andersson, H.I., Halden, R. and Glomsaker, T. (2000) Effects of surface irregularities on flow resistance in differently shaped arterial stenoses. Journal of Biomechanics, 33(10), 1257-1262.

[21] Yakhot, A., Grinberg, L. and Nikitin, N. (2005). Modeling rough stenoses by an immersed-boundary method. Journal of Biomechanics, 38(5), 1115-1127.

[22] Sarifuddin, Chakravarty, S., Mandal, P.K. and Andersson, H.I. (2009). Mass transfer to blood flowing through arterial stenosis. Zeitschrift für Angewandte Mathematik und Physik, 60(2), 299-323.

[23] Sarifuddin, Chakravarty, S. and Mandal, P.K. (2013). Physiological flow of shear-thinning viscoelastic fluid past an irregular arterial constriction. Korea-Australia Rheology Journal, 25(3),163-174.

[24] Sarifuddin, Chakravarty, S. and Mandal, P.K. (2014). Numerical simulation of Casson fluid flow through differently shaped arterial stenoses. Zeitschrift für angewandte Mathematik und Physik, 65(4), 767-782.

[25] Ne'mati, S.M.A., Ghassemi, M. and Shahidian, A. (2017). Numerical Investigation of Drug Delivery to Cancerous Solid Tumors by Magnetic Nanoparticles Using External Magnet. Transport in Porous Media, 119, 461–480.

[26] Spiridonova, T.I., Tverdokhlebov, S.I. and Anissimov, Y.G. (2019). Investigation of the size distribution for diffusion-controlled drug release from drug delivery systems of various geometries. Journal of Pharmaceutical Sciences, 108(8), 2690–2697.

[27] Kashkooli, F. M.,Soltani, M., Rezaeian, M., Meaney, C., Hamedi, M. H., Kohandel, M. (2020). Effect of vascular normalization on drug delivery to different stages of tumor progression: In-silico analysis. Journal of Drug Delivery Science and Technology, 60, 101989.

[28] König, A. and Klauss, V. (2007). Virtual histology. Heart, 93(8), 977-982.

[29] Mandal, P.K., Sarifuddin and Kolachalama, V.B.(2016). Computational model of drug-coated balloon delivery in a patient-specific arterial vessel with heterogeneous tissue composition. Cardiovascular Engineering and Technology, 7(4), 406-419.

[30] Harlow, F.H. and Welch, J.E. (1965). Numerical calculation of time-dependent viscous incompressible flow of fluid with free surface. The Physics of Fluids, 8(12), 2182-2189.

[31] Taylor,M. G. (1959). The influence of the anomalous viscosity of blood upon its oscillatory flow. Physics in Medicine and Biology, 3(3),273-290.

[32] Mandal, A. P., Sarifuddin and Mandal, P. K. (2015). An unsteady analysis of arterial drug transport from half-embedded drug-eluting stent. Applied Mathematics and Computation, 266, 968-981.

[33] Welch, J. E., Harlow, F. H., Shannon, J. P. and Daly, B. J. (1966). The MAC method, Los Alamos Scientifc Lab. Report LA 3425.

[34] Hirt, C. W. (1968). Heuristic stability theory for finite difference equations, Journal of Computational Physics, 2, 339-355.

[35] Markham, G. and Proctor, M. V. (1983). Modifications to the two-dimensional incompressible fluid flow code zuni to provide enhanced performance. CEGB Report TPRD= L, vol. 63, p. M82.

[36] Huang, Z. J. and Tarbell, J. M. (1997). Numerical simulation of mass transfer in porous media of blood vessel walls. American Journal of Physiology-Heart and Circulatory Physiology, 273(1), H464-H477

[37] Creel, C. J., Lovich, M. A. and Edelman, E. R. (2000). Arterial paclitaxel distribution and deposition. Circulation Research, 86(8), 879-884.

[38] Strikwerda, J.C. (2004). Finite Difference Schemes and Partial Differential Equations, vol. 88. SIAM, Philadelphia.

[39] Asakura, T., and Karino, T. (1990). Flow patterns and spatial distribution of atherosclerotic lesions in human coronary arteries. Circulation Research, 66(4), 1045-1066.

[40] Saltzman, W. M. (2001). Drug delivery: engineering principles for drug therapy. Oxford University Press.

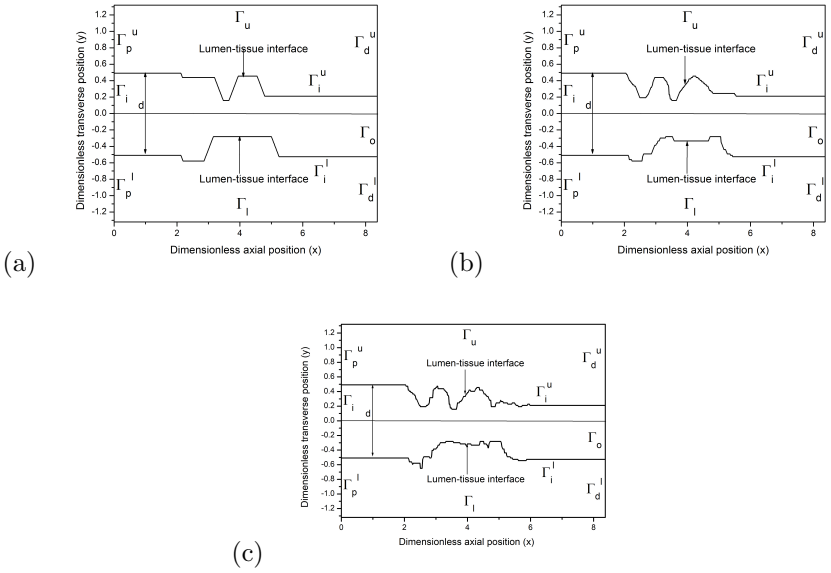

Figure 1: Computational domain, (a) Toy model, (b) Smooth model, (c) Original model, outline of the geometry derived from an IVUS image of a patient-specific atherosclerotic artery [28].

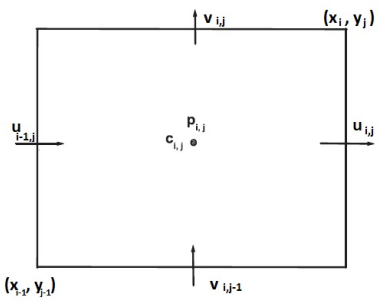

Figure 2: A typical MAC cell

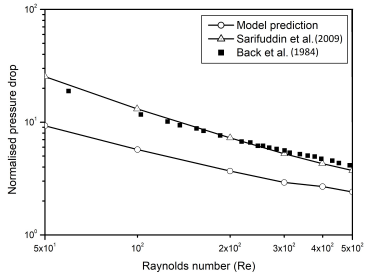

Figure 3: Comparison of normalized pressure drop across an irregular stenosis.

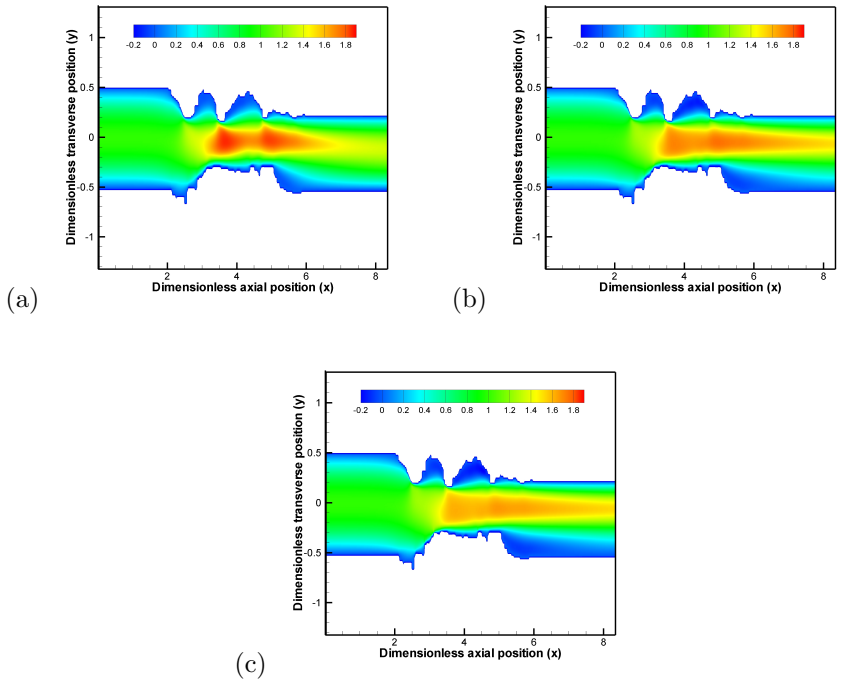

Figure 4: Longitudinal velocity contour, (a)$Re = 100$, (b)$Re = 300$, (c) $Re = 500$.

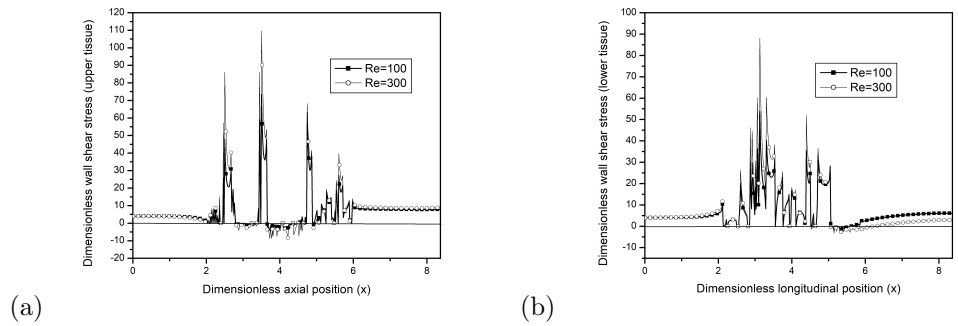

Figure 5: Variation of the wall shear stress along asymetrical atherosclerotic stenosis, (a) upper tissue, (b) lower tissue.

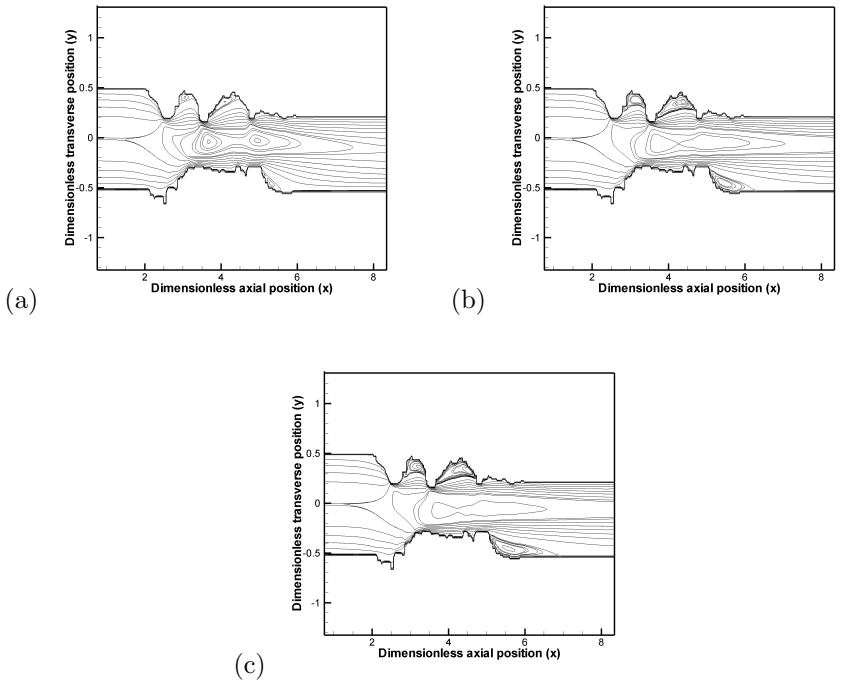

Figure 6: Variation of streamlines,(a)$Re = 100$, (b)$Re = 300$, (c)$Re = 500$.

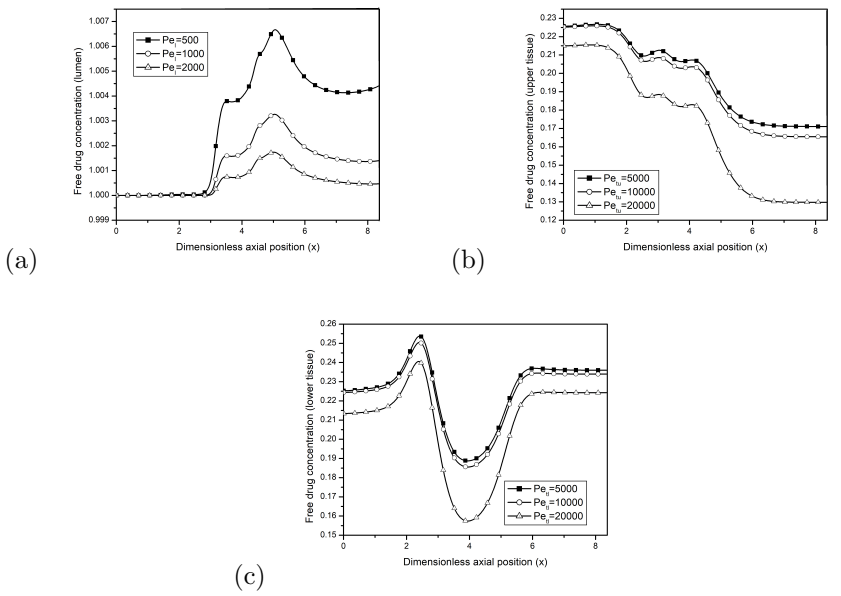

Figure 7: Axial variation of the local concentration of drug for different Peclet numbers, (a) lumen at $y = -0.2$, (b) upper tissue at $y = 1.15$, (c) lower tissue at $y = -1.15$.

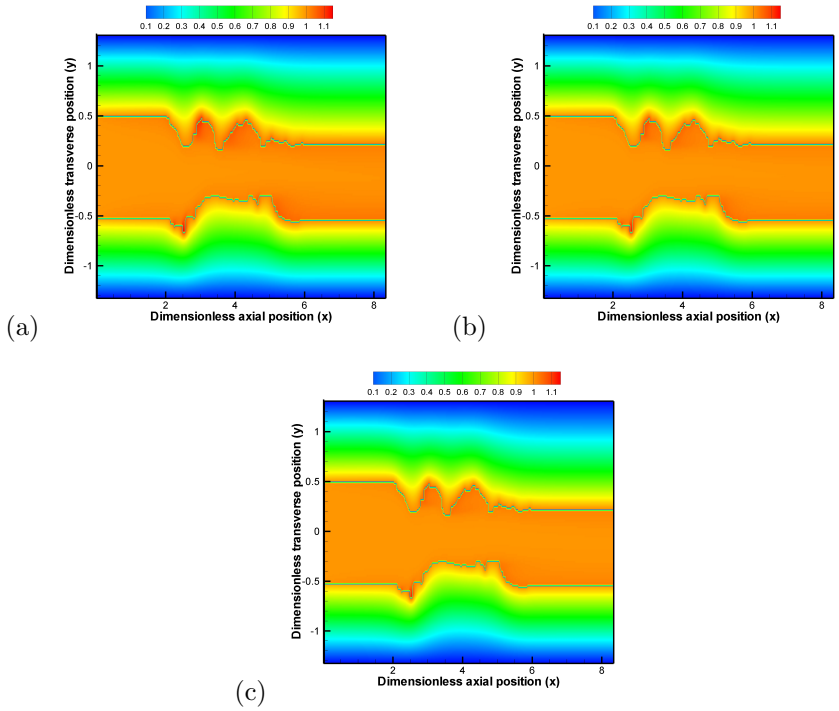

Figure 8: Spatiotemporal variation of drug concentration for different Peclet numbers ($Pe_{tu} = Pe_{tl} = 10 \times Pe_l$), (a) $Pe_l = 500$, (b)$Pe_l = 1000$, (c) $Pe_l = 2000$.

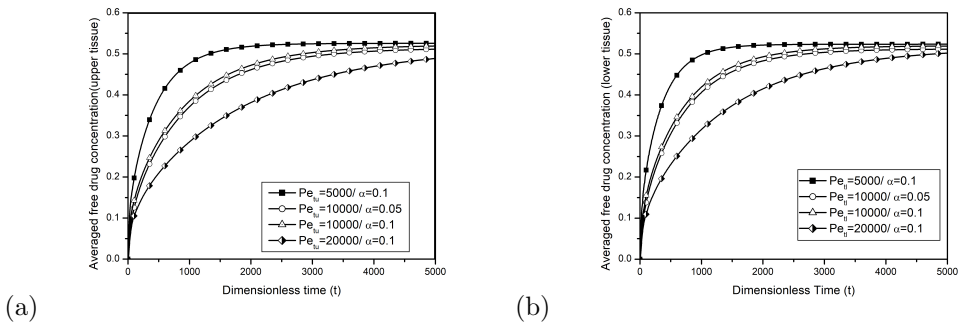

Figure 9: Temporal variation of dimensionless averaged concentration for different Peclet numbers and porosities, (a) upper tissue, (b) lower tissue.

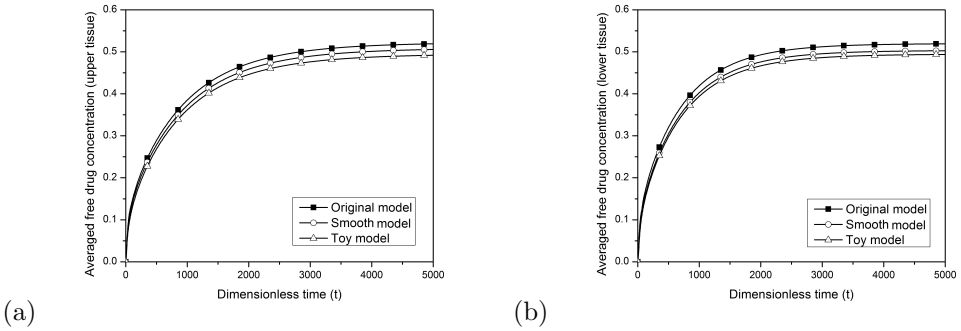

(a) (b)

Figure 10: Temporal variation of dimensionless averaged concentration for various geometrical models ($Pe_l = 1000, Pe_{tu} = Pe_{tl} = 10000, Re = 300, \alpha = 0.1$), (a) upper tissue, (b) lower tissue.

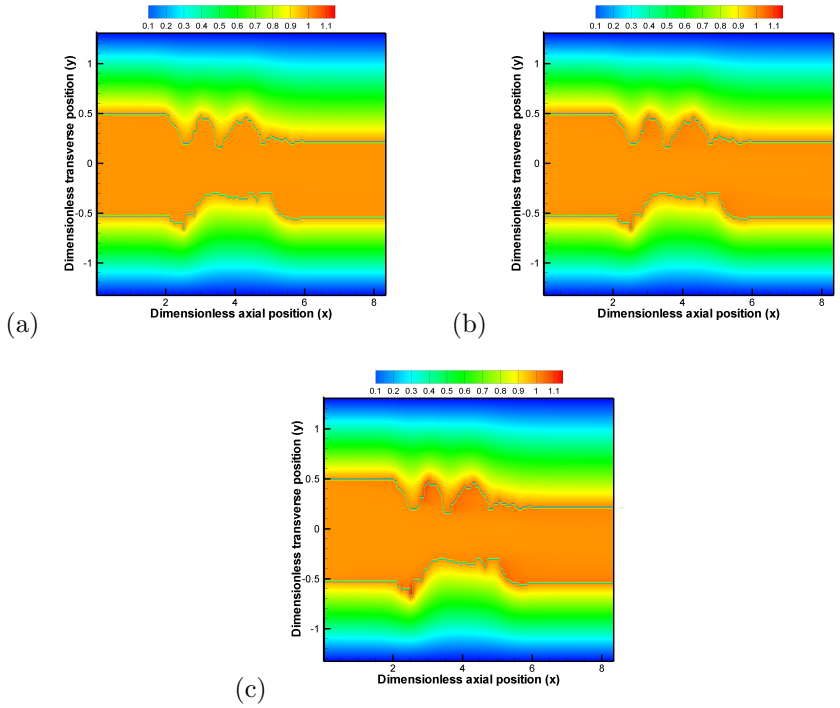

(a) (b) (c)

Figure 11: Spatiotemporal variation of drug concentration for different porosities ($Pe_l = 1000, Pe_{tu} = Pe_{tl} = 10000$), (a) $\alpha = 0.01$, (b) $\alpha = 0.05$, (c) $\alpha = 0.1$.

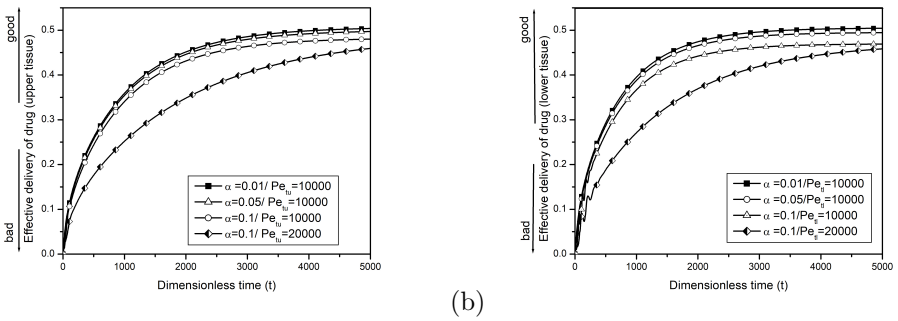

(a) (b)

Figure 12: Influence of Peclet number and porosity on the effectiveness of delivery, (a) upper tissue, (b) lower tissue.

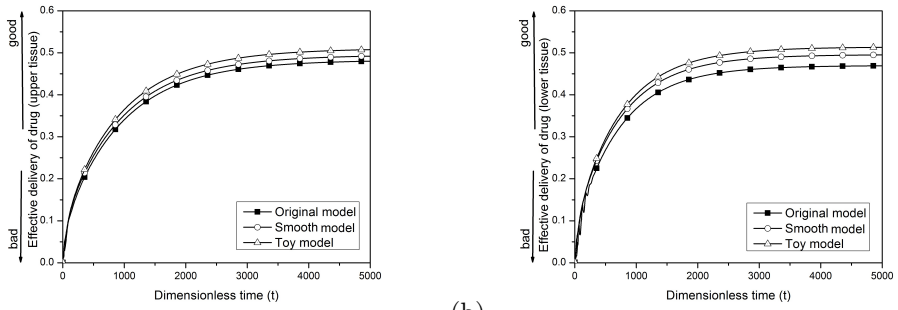

(a) (b)

Figure 13: Influence of surface roughness on the effectiveness of delivery ($Pe_l = 1000, Pe_{tu} = Pe_{tl} = 10000, Re = 300, \alpha = 0.1$), (a) upper tissue, (b) lower tissue.